Received: 30 December 2023 | Revised: 17 May 2024 | Accepted: 30 June 2024

DOI: 10.1002/cnm.3846

APPLIED RESEARCH

WILEY

Computational haemodynamics for pulmonary valve replacement by means of a reduced fluid-structure interaction model

Elisabetta Criseo[1,2] | **Ivan Fumagalli**[3] | **Alfio Quarteroni**[3,4] | **Stefano Maria Marianeschi**[5] | **Christian Vergara**[1]

[1]LaBS, Dipartimento di Chimica, Materiali e Ingegneria Chimica, Politecnico di Milano, Milan, Italy

[2]Centro Cardiologico Monzino IRCCS, Milan, Italy

[3]MOX, Dipartimento di Matematica, Politecnico di Milano, Milan, Italy

[4]Institute of Mathematics, École Polytechnique Fédérale de Lausanne, Lausanne, Switzerland

[5]Cardiac Surgery, ASST Grande Ospedale Metropolitano Niguarda, Milan, Italy

Correspondence
Ivan Fumagalli, MOX, Dipartimento di Matematica, Politecnico di Milano, piazza Leonardo da Vinci 32, Milan 20133, Italy.
Email: ivan.fumagalli@polimi.it

Funding information
European Union–NextGenerationEU; European Research Council (ERC); Italian Ministry of University and Research (MIUR); Italian Ministry of Health

Abstract

Pulmonary valve replacement (PVR) consists of substituting a patient's original valve with a prosthetic one, primarily addressing pulmonary valve insufficiency, which is crucially relevant in Tetralogy of Fallot repairment. While extensive clinical and computational literature on aortic and mitral valve replacements is available, PVR's post-procedural haemodynamics in the pulmonary artery and the impact of prosthetic valve dynamics remain significantly understudied. Addressing this gap, we introduce a reduced Fluid–Structure Interaction (rFSI) model, applied for the first time to the pulmonary valve. This model couples a three-dimensional computational representation of pulmonary artery haemodynamics with a one-degree-of-freedom model to account for valve structural mechanics. Through this approach, we analyse patient-specific haemodynamics pre and post PVR. Patient-specific geometries, reconstructed from CT scans, are virtually equipped with a template valve geometry. Boundary conditions for the model are established using a lumped-parameter model, fine-tuned based on clinical patient data. Our model accurately reproduces patient-specific haemodynamic changes across different scenarios: pre-PVR, six months post-PVR, and a follow-up condition after a decade. It effectively demonstrates the impact of valve implantation on sustaining the diastolic pressure gradient across the valve. The numerical results indicate that our valve model is able to reproduce overall physiological and/or pathological conditions, as preliminary assessed on two different patients. This promising approach provides insights into post-PVR haemodynamics and prosthetic valve effects, shedding light on potential implications for patient-specific outcomes.

KEYWORDS

image-based computational fluid dynamics, patient-specific analysis, pulmonary valve replacement, reduced fluid-structure interaction, tetralogy of Fallot

1 | INTRODUCTION

Valve replacement is a surgical treatment extensively used on patients with advanced valvular heart disease; it consists in the replacement of the patient's native valve with a prosthetic one.[1,2] In the clinical literature, the most studied procedures are aortic and mitral valve replacement[3–7]; however, valve replacement is an option also in the case of pulmonary valve pathologies and research about this procedure is increasing. The necessity for pulmonary valve replacement (PVR) is mainly linked to Congenital Heart Diseases (CHDs) that can present valvular malformations or involve the complete absence of a valve.

One of the most studied CHDs leading to PVR is the Tetralogy Of Fallot (TOF), which has an incidence of 3–5 every 10,000 newborns and accounts for 7%–10% of all congenital malformations.[8] This pathology consists in a tetrad of heart defects involving the ventricles, the ventricular septum, the Right Ventricle Outflow Tract (RVOT) and the aorta. The repair of the defects, especially the intervention on the RVOT, impacts also on pulmonary valve morphology, thus often yielding pulmonary regurgitation.[9–11] In most cases, this translates to the necessity of a subsequent PVR, as indicated by clinical guidelines.[12] Indeed, although pulmonary regurgitation is often well tolerated by patients, a long-term effect of this condition can be an increase in the volume load to the right ventricle and consequently its dilation, which then increases the risk of arrhythmias.[9] Another example of a surgical procedure leading to the need for a PVR is the Ross procedure, that is the substitution of the aortic valve with a pulmonary valve autograft, performed in the presence of an anomaly in the aortic valve morphology or function.[13] Consequently, the patient is left with a valveless conduit at the RVOT, leading to pulmonary insufficiency. Again, this condition must be treated with PVR to avoid an increased risk of arrhythmia and heart failure.

Mathematical and numerical models have been increasingly used to study pathologies and support clinical research, providing quantitative analyses of the mechanisms characterising the cardiovascular system. Pulmonary and systemic circulation can be mathematically modelled using different approaches. Lumped-Parameter Models (LPMs) describe, through a system of ordinary differential equations, the time evolution of the space-averaged flow rate and pressure in the compartments in which the cardiovascular system is divided.[14–16] This allows having a simple model which provides quantitative information about flow rate and pressure in the specific district of interest. In a clinical framework, this approach can be extremely resourceful since it is not computationally demanding and can be used to replicate the effect on the haemodynamics of different therapeutic approaches.[17–19] An alternative computationally efficient representation of haemodynamics is based on one-dimensional (1D) models. These models are able to reproduce waveforms of flow and pressure comparable both to physiological and pathological ones, as showed by Boileau, et al.[20] However, they do not allow having a detailed description of the local fluid dynamics with a possible reconstruction, for example, of wall shear stresses. Finally, three-dimensional models (3D) describe the haemodynamics with a higher degree of detail with respect to LPM and 1D models. Standalone 3D models of the pulmonary artery have been extensively used within the framework of Computational Fluid Dynamics (CFD) to analyse how haemodynamics vary with respect to physiological[21] and pathological settings, such as pulmonary hypertension[22] and congenital heart diseases,[23] but also as a consequence of surgical procedures.[24,25] However, these models are not able to describe the interactions between local haemodynamics and systemic circulation. To this aim, both 1D and 3D models could be coupled with 0D models.[26–29] Specifically, coupling 3D and 0D models has been adopted for the pulmonary circulation as a way of reducing the computational cost of the numerical simulation while still describing the complex relations between different compartments of the cardiovascular system.[30]

The mathematical models described above could be further improved by taking into account the interaction between the fluid and the surrounding structures, namely adopting a Fluid-Structure Interaction (FSI) approach. The interaction of the fluid with the arterial wall has been studied in a healthy setting[31,32] but also in the pathological framework of pulmonary arterial hypertension[33,34]; however, to our knowledge, there is a lack of studies reporting the FSI modelling of the pulmonary valve.

This study has two main objectives:

1. The development and calibration of a *reduced FSI model*, consisting in the coupling between a 3D model of the pulmonary artery and a one-degree-of-freedom mechanical model for the valve.
2. The application of the developed model to the clinical case of two patients who underwent the replacement of the pulmonary valve. For each of them, we modelled three scenarios to compare pre-implantation, post-implantation, and follow-up conditions.

The main novelty of this study is the extension of the reduced FSI model proposed by Fumagalli, et al.[35] to the pulmonary valve and its application to a patient-specific study. This model allows to reproduce the haemodynamics influenced by the presence of the valve that moves immersed in the fluid. To our knowledge, this is the first time that this kind of model has been applied to the study of pulmonary valve replacement. Moreover, since the study in this work is patient-specific, it allows to assess the applicability of the model to clinical conditions.

The paper has the following outline. In Section 2, we describe the mathematical methods and numerical models used. In Section 3.1 we discuss the clinical scenarios and the calibration of the models, whereas in Section 3.2 the geometry reconstruction and mesh generation processes are detailed. Finally, in Section 4 we present the results of the model application on two patients and we discuss the significance of the findings.

2 | MODELS AND METHODS

In this section, we want to outline the reduced Fluid-Structure Interaction (rFSI) model used in this study, which is based on the coupling between a 3D pulmonary artery model and a reduced pulmonary valve model where the opening is described by a single degree of freedom. We start by describing the continuous problems, consisting in the 3D blood flow dynamics, the one-degree-of-freedom valve mechanical model, and their coupling (Section 2.1). Then, we proceed by defining the corresponding numerical approximations in time and space (Section 2.2). Finally, we discuss the boundary conditions for the 3D problem, provided by a lumped-parameter model of the cardiocirculatory system (Section 2.3).

2.1 | Reduced fluid-structure interaction model

This mathematical model aims to describe the haemodynamics in the pulmonary artery, from the Right Ventricle Outflow Tract (RVOT), where the pulmonary valve is located, to the main branches of the right and left pulmonary arteries.

The choice of a rigid wall model for blood fluid dynamics, defined by using Navier–Stokes equations, is a consequence of the decision to neglect the artery wall compliance since the pulmonary artery is characterised by low pressure and small deformations. This is a widely accepted hypothesis, despite a slight overestimation of the Wall Shear Stress (WSS) is introduced.[36] Furthermore, as commonly accepted, the blood is modelled as a homogeneous, Newtonian and incompressible fluid, due to its composition and due to the fact that we are analysing haemodynamics in a large vessel, namely the pulmonary artery.[37,38]

Referring to Figure 1, top-left, we denote the fixed pulmonary artery domain by Ω, the artery wall by Γ_{wall}, the inlet/outlet sections by Γ_{in}/Γ_{out}, and the moving immersed valve surface by Γ_t. In this domain, the strong formulation of the problem reads:

Given the initial blood velocity $\mathbf{u}(t,\mathbf{x}) = \mathbf{0}$ at $t = 0$, for each time $t > 0$, find the blood velocity $\mathbf{u}$ and the blood pressure p, such that:

$$\begin{cases} \rho\dfrac{\partial \mathbf{u}}{\partial t} + \rho(\mathbf{u}\cdot\nabla)\mathbf{u} - \nabla\cdot\mathbf{T}_F + \dfrac{R}{\varepsilon}(\mathbf{u} - \alpha\mathbf{u}_\Gamma)\delta_{\Gamma_t,\varepsilon} = \mathbf{0} & in\ \Omega, \\ \nabla\cdot\mathbf{u} = 0 & in\ \Omega, \end{cases} \tag{1}$$

with $\mathbf{T}_F(\mathbf{u},p) = -p\mathbf{I} + \left(\mu + \mu_{sgs}\right)(\nabla\mathbf{u} + \nabla\mathbf{u}^T)$ the Cauchy stress tensor. The system is completed with no-slip conditions on Γ_{wall} and boundary conditions on Γ_{in} and Γ_{out} coming from a lumped-parameter model, see Section 2.3. In the Cauchy stress tensor, the presence of the sub-grid viscosity $\mu_{sgs} = \mu_{sgs}(\mathbf{u})$ is related to the adoption of the Large Eddy Simulation (LES) σ-model, successfully used to capture transitions to turbulence in haemodynamics.[39–41]

Notice that the presence of the valve is considered by adopting the Resistive Immersed Implicit Surface (RIIS) method,[42–44] which implies the addition of a resistive penalty term $\frac{R}{\varepsilon}(\mathbf{u} - \alpha\mathbf{u}_\Gamma)\delta_{\Gamma_t,\varepsilon}$ to the momentum balance equation. This includes the ratio between a resistance R, which acts as the penalty parameter, and the thickness ε of the leaflets. We remark that the resistive term has support only in a narrow layer around Γ_t, representing the moving valve leaflets surface; in the equation, this is described by the smoothed Dirac delta $\delta_{\Gamma_t,\varepsilon} = (1 + \cos(\pi\varphi/\varepsilon))/(2\varepsilon)$, where φ is the distance from the valve surface Γ_t. This term has the aim of enforcing the blood velocity $\mathbf{u}$ to be equal to a given field $\alpha\mathbf{u}_\Gamma$

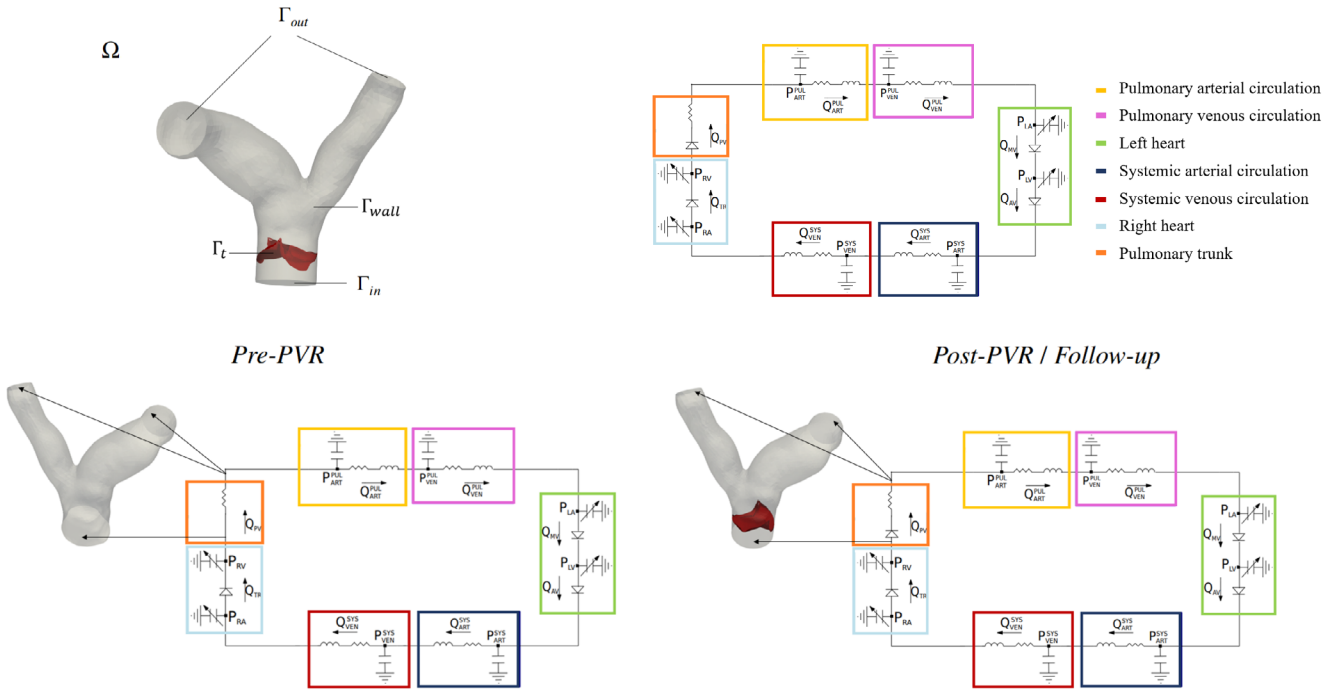

FIGURE 1 Top-left: Schematic representation of the domain Ω, of the physical and artificial boundaries $\Gamma_{wall}, \Gamma_{in}, \Gamma_{out}$, and of the pulmonary valve surface Γ_t; Top-right: Schematic representation of the lumped-parameter model of the whole circulation; Bottom: Lumped-parameter model used for the *Pre-PVR* scenario (left) and for the *Post-PVR* and *Follow-up* scenarios (right).

in proximity of the leaflets surface, $\alpha \in [0,1]$ being a parameter to be properly selected to enhance stability (see Section 4.1).

A mechanical model of the valve, suitably coupled with the blood dynamics problem (1), is required to obtain the current valve configuration Γ_t and the valve surface velocity $\mathbf{u}_\Gamma$. The one-degree-of-freedom (1-DoF) mechanical model introduced by Fumagalli, et al.[35] is chosen in order to reduce the computational effort demanded by the solution of a whole 3D FSI model, while still taking into account the presence of the valve and its encumbrance in the RVOT. Specifically, we describe the valve configuration by a single unknown variable $c = c(t)$, representing the opening fraction of the valve itself. As represented in Figure 2, the current valve configuration $\Gamma_t = \left\{\mathbf{x} = \widehat{\mathbf{x}} + \mathbf{d}_\Gamma(t,\mathbf{x}) : \widehat{\mathbf{x}} \in \widehat{\Gamma}\right\}$ is then defined in terms of the closed configuration $\widehat{\Gamma}$ and the following displacement function:

$$\mathbf{d}_\Gamma(t,\widehat{\mathbf{x}}) = c(t)\mathbf{g}(\widehat{\mathbf{x}}), \tag{2}$$

where, here and in what follows, quantities with the $\widehat{\cdot}$ refer to the reference configuration, $\mathbf{d}_\Gamma : [0,T] \times \widehat{\Gamma} \to \mathbb{R}^3$ denotes the displacement of the leaflet and $\mathbf{g} : \widehat{\Gamma} \to \mathbb{R}^3$ is the displacement between the fully closed and fully open configurations, which are known from imaging, see Section 3.2. We point out that $\mathbf{g}$ is constructed considering each leaflet separately, and that no self-intersections occur for any intermediate configuration $\Gamma_\phi = \left\{\mathbf{x} = \widehat{\mathbf{x}} + \phi\mathbf{g}(\widehat{\mathbf{x}}) : \widehat{\mathbf{x}} \in \widehat{\Gamma}\right\}, \phi \in [0,1]$.

Thus, the 1-DoF structure model in the unknown c reads as follows[35]:

$$\ddot{c} = -\beta\dot{c} + \frac{\displaystyle\int_{\Gamma_t} \mathbf{f}(t,\mathbf{x}) \cdot \mathbf{n}_\Gamma(\mathbf{x}) d\mathbf{x} - \gamma \int_{\Gamma_t} \left[H(\mathbf{x}) - \hat{H}(\hat{\mathbf{x}}) - \chi\right] d\mathbf{x}}{\displaystyle\int_{\Gamma_t} \rho_\Gamma \mathbf{g}(\hat{\mathbf{x}}) \cdot \mathbf{n}_\Gamma(\mathbf{x}) d\mathbf{x}}, \tag{3}$$

where H is the leaflets curvature, $\mathbf{n}_\Gamma$ is the normal to Γ_t, β is the damping coefficient, γ is the stiffness, ρ_Γ is the surface density, and χ is a suitable coefficient ensuring that the curvature term is responsible for the valve closure. This ordinary differential equation is completed by suitable initial conditions on $c(0)$ and $\dot{c}(0)$. In this study, we assume that the valve is initially closed and still: $c(0) = 0$ and $\dot{c}(0) = 0$.

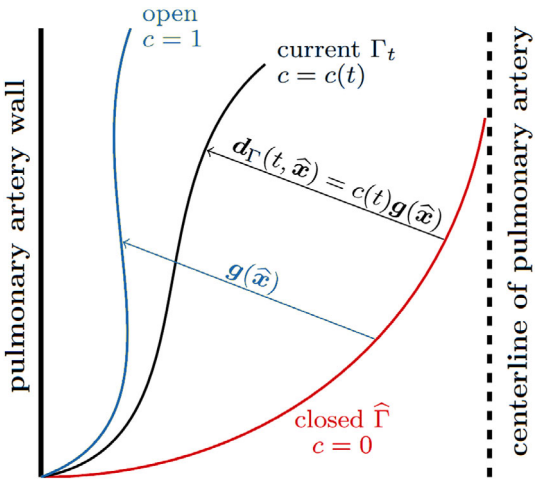

FIGURE 2 Schematic representation of the 1-DoF model for the valve. The current position Γ_t of the valve (black) is determined from its fully closed (red) and fully open (green) configuration, in terms of the opening coefficient $c(t)$, see (2).

To couple the 3D fluid model (1) and the 1-DoF valve model (3) we need the kinematic and dynamic coupling conditions. The kinematic condition is represented by the resistive penalty term $\frac{R}{\varepsilon}(\mathbf{u} - \alpha\mathbf{u}_\Gamma)\delta_{\Gamma_t,\varepsilon}$ in (1), with $\mathbf{u}_\Gamma = \mathbf{d}_\Gamma = \dot{c}\mathbf{g}$. The dynamic condition is given by the force balance $\mathbf{f} = \mathbf{T}_F\mathbf{n}_\Gamma$ on Γ_t. Here and in (3), greek letters indicate parameters that need to be suitably calibrated, see Section 3.3.2.

This coupling leads to the following reduced[i] FSI (rFSI) problem:

Given the valve displacement $\mathbf{g}$ mapping the fully closed configuration to the fully open one, find $\mathbf{u}, p, c, z$ for each $t \in (0, T]$, such that:

$$\text{Structure problem} \begin{cases} \dot{c} = z, \\ \dot{z} = \eta(\Gamma_t, \mathbf{f}, H, c, z; \beta, \gamma, \chi, \rho_\Gamma, \mathbf{g}), \end{cases} \tag{4a}$$

$$\text{Coupling} \begin{cases} \Gamma_t = \left\{\widehat{\mathbf{x}} + c\,\mathbf{g}(\widehat{\mathbf{x}}) : \widehat{\mathbf{x}} \in \widehat{\Gamma}\right\}, \\ \mathbf{u}_\Gamma = \dot{c}\,\mathbf{g} \quad on\ \Gamma_t, \\ \mathbf{f} = \mathbf{T}_F\mathbf{n}_\Gamma \quad on\ \Gamma_t, \end{cases} \tag{4b}$$

$$\text{Fluid problem} \begin{cases} \rho\dfrac{\partial \mathbf{u}}{\partial t} + \rho(\mathbf{u}\cdot\nabla)\mathbf{u} - \nabla\cdot\mathbf{T}_F + \dfrac{R}{\varepsilon}(\mathbf{u} - \alpha\mathbf{u}_\Gamma)\delta_{\Gamma_t,\varepsilon} = \mathbf{0} & in\ \Omega, \\ \nabla\cdot\mathbf{u} = 0 & in\ \Omega, \end{cases} \tag{4c}$$

where the structure problem is written as a system of first-order ordinary differential equations with $\eta(\Gamma_t, \mathbf{f}, H, c, z; \beta, \gamma, \chi, \rho_\Gamma, \mathbf{g})$ as the right-hand side of (3).

2.2 | Numerical approximation

The rFSI model (4) is discretised both in time and space. We introduce a uniform partition of the time interval $[0, T]$ with step-size Δt; the partition has nodes $\{t^n\}_{n=0}^N$ and the step-size is defined as $\Delta t = T/N$. Considering a generic function $v(t)$, v^n indicates the approximation of $v(t^n)$. Therefore, the time-discretised rFSI problem reads:

$$\text{Structure problem} \left\{ \begin{bmatrix} c^n \\ z^n \end{bmatrix} = \tilde{\eta}\left(\Gamma^{n-1}, \mathbf{f}^{n-1}, H^{n-1}, c^{n-1}, z^{n-1}; \beta, \gamma, \chi, \rho_\Gamma, \mathbf{g}\right), \right. \tag{5a}$$

$$\text{Kinematic coupling} \begin{cases} \Gamma^n = \left\{ \widehat{\mathbf{x}} + c^n \mathbf{g}(\widehat{\mathbf{x}}) \ : \ \widehat{\mathbf{x}} \in \widehat{\Gamma} \right\}, \\ \mathbf{u}_\Gamma^n = \dfrac{c^n - c^{n-1}}{\Delta t} \mathbf{g} \text{ on } \Gamma^n, \end{cases} \tag{5b}$$

$$\text{Fluid problem} \begin{cases} \rho \dfrac{\mathbf{u}^n - \mathbf{u}^{n-1}}{\Delta t} + \rho(\mathbf{u}^{n-1} \cdot \nabla)\mathbf{u}^n - \nabla \cdot \mathbf{T}_F^n + \dfrac{R}{\varepsilon}(\mathbf{u}^n - \alpha \mathbf{u}_\Gamma^n)\delta_\varepsilon^n = 0 & in\ \Omega, \\ \nabla \cdot \mathbf{u}^n = 0 & in\ \Omega. \end{cases} \tag{5c}$$

$$\text{Dynamic coupling} \left\{ \mathbf{f}^n = \mathbf{T}_F^n \mathbf{n}_\Gamma^n \quad \text{on } \Gamma^n. \right. \tag{5d}$$

where $\tilde{\boldsymbol{\eta}}$ is defined by the discretisation of (4a) with the classical fourth-order, explicit Runge–Kutta method.[45]

The time discretisation for the 3D fluid model (5c) is carried out by means of the Backwards Differentiation Formula (BDF) of order 1 with a semi-implicit treatment for the non-linear term $\rho(\mathbf{u} \cdot \nabla)\mathbf{u}$ in (1). The space discretisation of the fluid problem is carried out by the Finite Element (FE) method of order 1 for both velocity and pressure with a SUPG-PSPG stabilisation.[46,47] As for the 1-DoF valve model, the assembly of the right-hand side $\tilde{\boldsymbol{\eta}}$ hinges upon the RIIS representation of the valve surface Γ^n and normal vector $\mathbf{n}_\Gamma^n$, as previously discussed.[35]

The fluid and structure models are then weakly (explicitly-in-time) coupled at each time step, meaning that the 3D fluid model and the 1-DoF structure model exchange information only once per time step. Specifically, at each t^n, the structure problem (5a) is solved by using the fluid interface force $\mathbf{f}^{n-1}$ taken from the previous time step, and the new interface position and velocity are computed using the kinematic coupling conditions (5b). Then, the fluid problem (5c) is solved accordingly. This scheme is summarised in Algorithm 1:

Algorithm 1 has been solved in the computational fluid dynamics module life^x-cfd[48] of life^x,[49,50] a high-performance library for the finite element simulations of multiphysics, multiscale, and multidomain problems, developed within the iHeart project (https://iheart.polimi.it/), at the MOX laboratory of the Department of Mathematics—Politecnico di Milano.

2.3 | Boundary conditions: lumped-parameters model of the circulation

In order to obtain suitable boundary conditions for the artificial boundaries $\Gamma_{in}, \Gamma_{out}$ of the 3D computational domain, we introduce a closed-loop Lumped-Parameters Model (LPM) of the whole circulatory system (Figure 1, top-right) as already proposed in literature,[30,51,52] which is solved once and for all before the starting of the 3D simulation (One-Way coupling). Previous works such as Marcinnò, et al.[30] show that, in terms of haemodynamics in the pulmonary artery, a One-Way coupling between the 3D model and the LPM produces substantially equivalent results to a Two-way coupling.

In this LPM we model the pulmonary valve as a non-ideal diode represented by a variable resistance $R = 10^b$, with b defined as:

ALGORITHM 1 SCHEME FOR THE SOLUTION OF THE rFSI MODEL

Given $\mathbf{u}_h^0, p_h^0, c^0$ and the initial surface Γ^0,

1: **for** $n = 1$ to N **do.**
2: Compute the fluid force $\mathbf{f}^{n-1}$ and the integrals that make up (3), in terms of $\mathbf{u}_h^{n-1}, p_h^{n-1}, \Gamma^{n-1}$;
3: Find c^n by advancing the 0D Equation (5a) with a step of the explicit fourth-order Runge–Kutta method;
4: Create the immersed surface Γ^n moving the previous configuration Γ^{n-1} by $\mathbf{d}_\Gamma^n - \mathbf{d}_\Gamma^{n-1} = (c^n - c^{n-1})\mathbf{g}$;
5: Compute the leaflets velocity $\mathbf{u}_\Gamma^n = \frac{c^n - c^{n-1}}{\Delta t} \mathbf{n}_{\Gamma,h}^n$;
6: Find $\left(\mathbf{u}_h^n, p_h^n\right)$ by solving the fluid problem (5c).
7: **end for**.

$$b = \log_{10} R_{min} \; + \; (\log_{10} R_{max} - \log_{10} R_{min}) \cdot \left[\frac{1}{2} + \frac{1}{\pi} \arctan\left(\frac{k\pi}{2} \left(P_{\mathrm{ART}}^{\mathrm{PUL}} - P_{\mathrm{RV}} \right) \right) \right],$$

so that R is a sigmoidal function smoothly transitioning from the resistance R_{min} (when the valve is open) to R_{max} (when the valve is closed), depending on the jump between the pulmonary artery pressure $P_{\mathrm{ART}}^{\mathrm{PUL}}$ and the right ventricle pressure P_{RV} indicated in Figure 1, top-right.[30] Notice that with this choice we are not able to model the valve opening/closing dynamics in the LPM.

Since the 3D model corresponds to the 0D pulmonary trunk district (orange in Figure 1, top-right), a possible choice for the boundary conditions on Γ_{in}, Γ_{out} are the following:

$$\begin{cases} \mathbf{T}_F(\mathbf{u}^n, p^n)\mathbf{n} = P_{RV}(t^n)\mathbf{n} & on\ \Gamma_{in}, \\ \mathbf{T}_F(\mathbf{u}^n, p^n)\mathbf{n} = P_{ART}^{PUL}(t^n)\mathbf{n} & on\ \Gamma_{out}, \end{cases} \tag{6}$$

where the solution of the LPM was found using the explicit fourth-order Runge–Kutta (RK) scheme. Notice that this choice, here and for the 1-DoF model, is motivated by the simplicity of such problems, which are in fact ODE systems, thus guaranteeing accuracy of the solution. Specifically, for LPM problems the explicit fourth order RK scheme has been already used in haemodynamics and in particular for the pulmonary circulation.[53] Instead, for the 3D fluid problem a first-order method in time is preferred to reduce computational complexity.

The LPM parameters are suitably tuned in order to adhere as much as possible to the values of the patients' available clinical data (see Section 3.3.1).

The LPM is solved in the library life^{x}.[49,50]

3 | RECONSTRUCTION PROCEDURE AND SCENARIOS OUTLINE

In order to carry out a patient-specific analysis of pulmonary artery haemodynamics, we rely on the study of two patients' clinical data. The patients' CT scans were provided by the Department of Cardiac Surgery of hospital ASST Grande Ospedale Metropolitano Niguarda, Milan, Italy. Ethical Review Board approval and informed consent from all patients were obtained.

The patients, P1 and P2, were left without a pulmonary valve for decades, after having undergone the Ross procedure in the treatment of their Tetralogy of Fallot. Then, they were subject to PVR, with the implantation of the *No-React® BioPulmonic™* valve, composed by porcine pulmonary leaflets surrounded by a bovine pericardium sleeve, which are mounted on a self-expandable Nitinol stent.[54]

We build the geometric configurations of both before (pre-implantation scenario) and after (post-implantation scenario) the PVR, together with a follow-up scenario after 9 years, to evaluate the impact of the prosthetic valve on haemodynamics. To this aim, in the following of this section we describe the building-up of the three computational scenarios (Section 3.1), the reconstruction of the 3D fluid domain from the patients' CT scans (Section 3.2), and the calibration of the valve parameters in the rFSI model and of the LPM parameters (Section 3.3).

3.1 | Computational scenarios

We introduce the three computational scenarios (Figure 1, bottom) used for each patient:

1. *Pre-PVR*: the pre-implantation scenario is characterised by the absence of the valve. Accordingly, in the rFSI model (5) we set $R = 0$, whereas in the LPM we set $R_{max} = R_{min} = 2.2 \cdot 10^{-2}\,\mathrm{mmHg \cdot s \cdot ml^{-1}}$. Notice that in this case the rFSI model is in fact a CFD model, due to the absence of the valve;
2. *Post-PVR*: the prosthetic valve is implanted, so we use the rFSI model (5) with $R = 10^4\,\mathrm{kg\,m^{-1}\,s^{-1}}$ and the LPM with $R_{max} >> R_{min}$ (specifically, $R_{max} = 7.5 \cdot 10^4\,\mathrm{mmHg \cdot s \cdot ml^{-1}}$ and $R_{min} = 2.2 \cdot 10^{-2}\,\mathrm{mmHg \cdot s \cdot ml^{-1}}$);
3. *Follow-up*: we have the same scenario as in Post-PVR, where, however, the LPM parameters are different to account for the evolution of the patients' conditions (see Section 3.3.1).

Notice that the calibration of the LPM and 1-DoF valve model for all scenarios (including R_{min}) is carried out by using patient-specific data (see Section 3.3). For the closed valve resistance R_{max} of the LPM we adopt the value proposed in Regazzoni, et al.[52]

3.2 | Geometries reconstruction

Pre-implantation CT scans are used to obtain patient-specific 3D pulmonary artery geometries for both P1 and P2. The segmentation process is carried out using VMTK.[55,56] The reconstructed geometries include multiple outlets and we use Paraview[57] and VMTK to remove secondary branches. The final geometries are composed of the pulmonary trunk and two outflow regions which correspond to the two branches originating from the first bifurcation of the pulmonary artery (see Figure 3, left).

The post-implantation cases, Post-PVR and Follow-up, are characterised by the same geometry, obtained from Pre-PVR geometries and virtually inserting the stent graft. Notice that the pulmonary trunk geometry is different from the Pre-PVR scenario due to the stent presence. The stent is modelled as a cylinder with the nominal length (20 mm) and diameter (29 mm) of the *No-React® BioPulmonic™* valve. This cylinder is positioned and oriented in accordance with the patient-specific position of the commissures reconstructed from post-implantation CT scans (Figure 3, right).

As for the pulmonary valve, the resolution of the CT scans does not allow the reconstruction of the leaflets. Thus, a template valve model by Zygote[58] is adapted to the stent geometry to obtain the valve closed configuration $\widehat{\Gamma}$. Afterwards, the open configuration is derived from the closed one by pure geometric deformation, opening the leaflets compatibly with the surrounding stent to have a physiological orifice area (see Figure 4). The prescribed deformation is then used in the rFSI model (5) as the variable $\mathbf{g}$.

The 3D fluid mesh generation is carried out in the same way for the Pre-PVR, Post-PVR and Follow-up scenarios. Specifically, we use a non-uniform mesh characterised by a cell diameter $h = 1.1$ mm in the pulmonary trunk and $h = 4.3$ mm at the outlets (Figure 5). This allowed us to have higher accuracy in the region where higher velocities and wall shear stresses are expected, and to properly capture the leaflets dynamics by the RIIS method.

The meshes used in this work are obtained after a mesh-independence study in the Pre-PVR scenarios where we checked that the Wall Shear Stress (WSS) differs by at most 2% when the mesh was refined by a 10% factor.

3.3 | Calibration procedure

In the following section we detail the calibration procedure both for the LPM and the 1-DoF valve model. Specifically, the LPM is calibrated utilising P1's patient-specific data we have at our disposal to obtain suitable boundary conditions (Section 3.3.1), while the 1-DoF model is calibrated employing literature data to reproduce a physiological dynamics of the valve (Section 3.3.2).

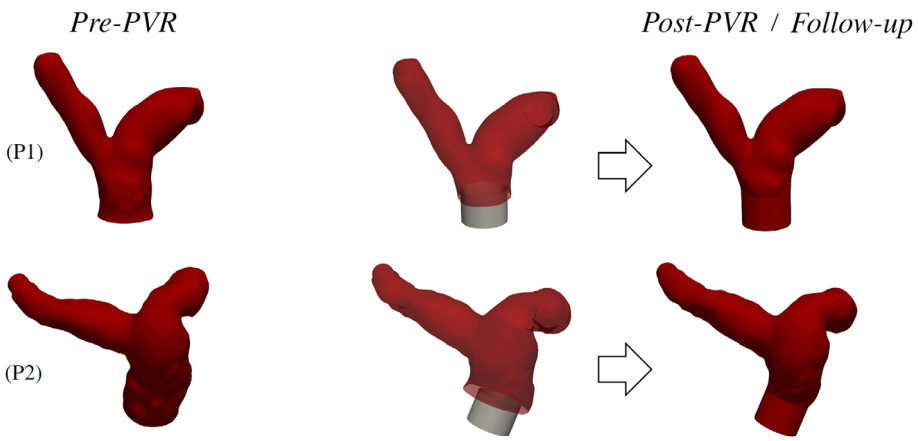

FIGURE 3 Reconstructed geometries used to build the three scenarios of both P1 and P2. Left: Pre-PVR as from image segmentation; Right: Virtual insertion of the PV stent to create the Post-PVR/Follow-up scenarios.

3.3.1 | Lumped-parameters models calibration

The LPMs calibration of all three scenarios relies on the use of P1's clinical data, see Table 1. Specifically, we create three different sets of calibrated LPM parameters, one for each scenario, and we use:

- The End-Systolic Volume (ESV), that is, the residual volume in the ventricle after the ejection of blood in the systolic phase;
- The End-Diastolic Volume (EDV), that is, the volume in the ventricle at the end of diastole;

the Ejection Fraction (EF), calculated as $\frac{EDV-ESV}{EDV}$.

Notice that the data measured 9 years after the PVR lie in physiological ranges found in the literature.[59]

In the process of calibration, the LPM parameters are iteratively changed until the simulated EF is characterised by a small difference with respect to the corresponding measured value. For the calibration of the Post-PVR and Follow-up LPMs, we use the data at 6 months and 9 years after the PVR, respectively (Table 1). For the Pre-PVR scenario, there was no available data describing the patient's condition before the surgery; thus, we use the Post-PVR EF, EDV and ESV to calibrate also the Pre-PVR LPM, since EF values typically do not change significantly six months after the surgery[60]; see the limitations in Section 5 for further discussion on this point.

Since only the ESV, EDV and EF of the patients are available, we conduct our calibration manually and only on a small subset of LPM parameters that are more strictly related to the haemodynamics in the pulmonary artery. Specifically, we assign the EDV of the right ventricle V_{RV} from P1's data and we calibrate the following parameters to match EF[30,52]:

- The elastances of the right heart: E_a, E_b;
- The RLC circuit describing the pulmonary arterial circulation, composed by the resistance R_{art}, the capacitance C_{art} and the inductance I_{art};

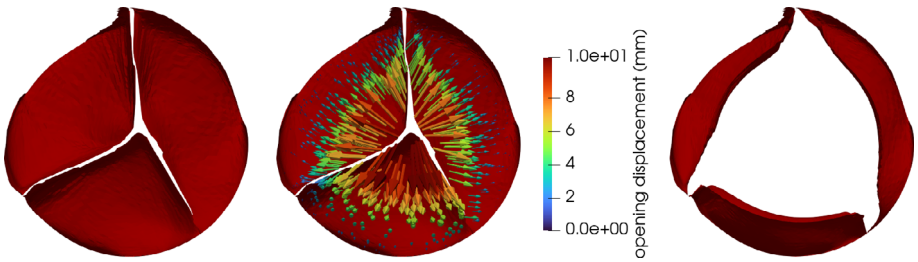

FIGURE 4 The closed configuration of the pulmonary valve (left), the displacement imposed to the leaflets surface to obtain the physiological open configuration from the closed one (centre) and the open configuration (right).

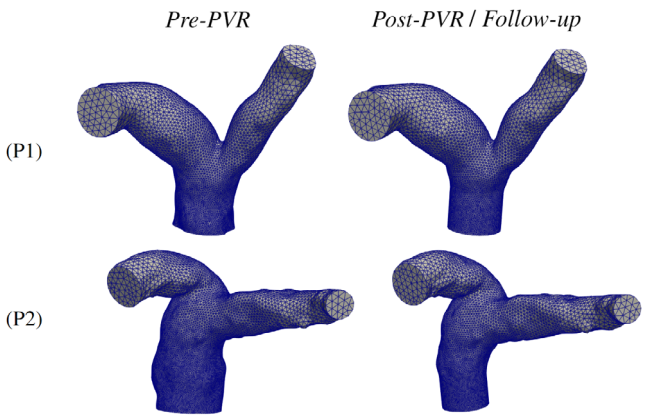

FIGURE 5 The meshes of P1 and P2 used in the three scenarios considered.

- The non-ideal diode representing the pulmonary valve, modelled by two resistances and an inductance: R_{max}, R_{min}, I_v.

The values of all the other LPM parameters are taken from Marcinnò, et al.[30] We also fix the right atrium EDV V_{RA} to the physiological value of 45 ml as reported in the literature.[61]

The values of the calibrated parameters reported in Table 2 allow to obtain EF (also reported in Table 2) very close to P1's measures in Table 1: in the Pre-PVR scenario we have a difference of 0.3%, in the Post-PVR scenario of 10%, and in the Follow-up scenario of 12.5%. Moreover, in Figure 6 we observe that the calibrated LPM reproduce Wiggers diagrams which are physiological for both the pulmonary and systemic circulation in the Follow-up scenario[62] and consistent with the patient conditions in the Pre-PVR scenario. The LPM systemic circulation attains physiological values also in the Pre-PVR scenario, consistently with no comorbidities being reported for the patients.

3.3.2 | Valve model calibration

In the Post-PVR and Follow-up scenarios, the 1-DoF model parameters are suitably set to achieve opening and closing times of the leaflets in accordance with the literature.[63,64] The valve model calibration implies the tuning of 5 parameters:

- The *damping coefficient* (β in Equation 3) associated with the leaflets velocity;
- The *stiffness coefficient* (γ in Equation 3), associated with the elastic forces;
- The *added curvature* (χ in Equation 3) parameter;
- The *surface density* (ρ_Γ in Equation 3), associated to the inertial properties of the leaflets;

TABLE 1 Clinical measurements of patient P1 for the calibration of the LPMs.

	6 months after PVR	9 years after PVR
ESV (ml)	105	58
EDV (ml)	165	110
EF%	35	47

TABLE 2 Calibrated parameters of the LPM, the initial volumes used for right ventricle V_{RV} and right atrium V_{RA}, and the EF value found by the numerical simulations of the circulation with the calibrated parameters for each scenario.

Used data (see Table 1)	Pre-PVR 6 months after PVR	Post-PVR 6 months after PVR	Follow-up 9 years after PVR
Right ventricle			
E_a (mmHg ml^{-1})	0.07	0.10	0.24
E_b (mmHg ml^{-1})	0.09	0.08	0.08
Pulmonary arterial circulation			
R_{art} (mmHg s ml^{-1})	0.05	0.05	0.07
C_{art} (ml mmHg^{-1})	7.0	7.0	8.0
I_{art} (mmHg s^2 ml^{-1})	5e-3	5e-3	5e-3
Pulmonary valve			
R_{max} (mmHg s ml^{-1})	2.2e-2	7.5e4	7.5e4
R_{min} (mmHg s ml^{-1})	2.2e-2	2.2e-2	2.2e-2
V_{RA} (ml)	45	45	45
V_{RV} (ml)	165	165	110
EF%	35.1	38.8	52.9

- The coefficient α introduced in the resistive penalty term in Equation (1).

The calibration aims at matching the opening and closing times of the leaflets with the values reported in the literature. Since the number of parameters of the valve model is relatively small, we adopted a manual calibration strategy for parameter tuning, considering separately the Post-PVR and Follow-up scenario. In this procedure, we observed that increasing γ mostly affects the *starting time* of the opening/closing phases, whereas the interplay of the others influences its duration (with different sensitivities). The calibrated values are reported in Table 3. In particular, in the calibration of coefficient α, the admissible values were restricted to obtain a numerically stable result.

With these calibrated parameters we obtain a valve dynamics close to the analysed literature[63,64]; we report in Table 4 the values obtained from the simulation, regarding the duration of opening and closing times (namely the transitions of the opening coefficient c from 0 to 1 and from 1 to 0), and the open-state duration (the period when c stays equal to 1) for P1. Notice that we make the assumption that the valve properties remain unaltered from the Post-PVR to the Follow-up, so the same calibrated parameters are used in both cases.

4 | RESULTS AND DISCUSSION

In this section we present and discuss the results of the 3D rFSI simulations in the three scenarios previously described (Section 3.1).

4.1 | Settings of the numerical experiments

The parameters of the rFSI model and LPM model are set according to the result of the calibration procedures reported in Section 3.3. We make the assumption that, since the model describes the same valve implanted in both patients, the calibrated valve parameters found for P1 can be applied also to the numerical simulations of P2. This approach yields acceptable values of valve opening and closure times also for P2: for example, the opening time is 66 and 46 ms in the Post-PVR and Follow-up scenarios, respectively.

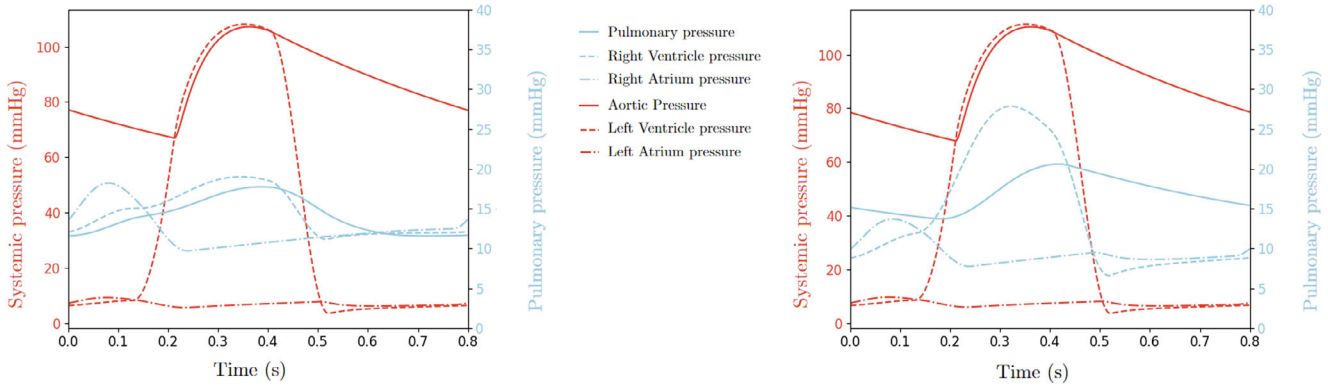

FIGURE 6 Wiggers diagrams from the calibrated LPM numerical simulations in the Pre-PVR (left) and Follow-up (right) scenarios.

TABLE 3 Calibrated parameters for the reduced structural valve model in the Post-PVR and follow-up scenarios.

Parameters	Values in Post-PVR/Follow-up scenarios
$\beta\,(\mathrm{s}^{-1})$	0.28
$\gamma\,(\mathrm{s}^{-2})$	0.13
$\chi\,(\mathrm{m}^{-1})$	0.24
$\rho_\Gamma\,(\mathrm{kg\,m}^{-2})$	106
$\alpha\,(-)$	0.075

TABLE 4 Computed timings of opening and closing of the simulated pulmonary valve dynamics both for the *Post* and *Follow-up* scenarios for P1.

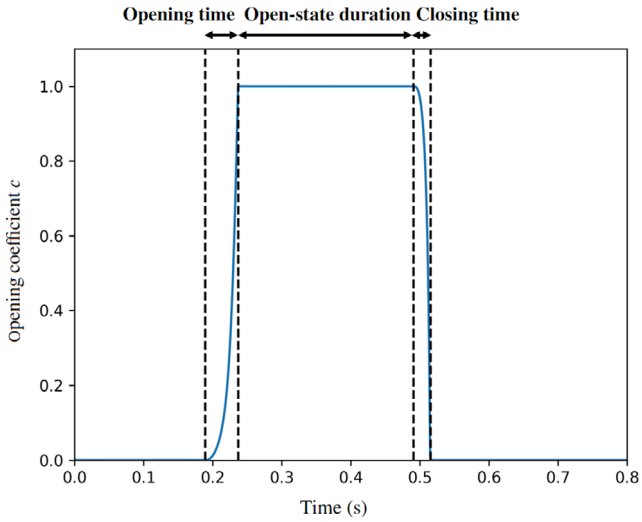

	Opening time (ms)	Open-state duration (ms)	Closing time (ms)
Post-PVR (P1)	104	336	47
Follow-up (P1)	47	254	23

Moreover, we set $\rho = 1.06 \cdot 10^3$ kg m^{-3}, $\mu = 3.5 \cdot 10^{-3}$ Pa s, $R = 10^4$ kg m $^{-1}$ s^{-1} and $\varepsilon = 1.8$ mm, and the coefficient α in (5c) is set to 0.075 in order to reproduce more physiological results and enhance stability. Indeed, by using $\alpha = 1$ (which would guarantee a fully consistent no-slip condition) we were not able to recover stable results. Notice that our choice is intermediate between the fully consistent and the quasi-static ($\alpha = 0$) conditions—in particular, close to the latter – thus formally violating the physical adherence of the blood to the valve. However, since the quasi-static assumption has been widely used in the literature,[65] we believe that our choice is acceptable. Also, the value of ε is chosen in order to satisfy the condition $\varepsilon > 1.5\ h$, necessary for the correct resolution of $\delta^n_{\varepsilon,h}$ in the resistive model.[43]

Regarding the time discretisation parameter, we set $\Delta t = 5 \cdot 10^{-4}$ s for both LPM and rFSI problems. This value is chosen after a convergence analysis showing that, by halving Δt, the quantities of interest do not change by more than 2%. This value of the time step also allows us to satisfy the stability conditions associated with the explicit coupling between the 3D fluid model and the 1-DoF structural valve model.

To obtain the boundary conditions (6) for the rFSI model, the LPM should reach a periodic state independent of the initial condition. To this aim, we run six cardiac cycles (period $T = 0.8$ s). Since the peak values of pressure at cardiac cycles 5 and 6 differ by less than 2%, we deem periodicity to be reached. Accordingly, only the sixth cycle is used to extract the pressure curves at the right ventricle and pulmonary artery compartments, to be prescribed at the inlet and outlets of the 3D model, respectively (Figure 7, top). In Figure 7, bottom, we display the corresponding pressure drops between inlet and outlets. As for the solution of the rFSI model, we simulate two cardiac cycles; the results shown in the next sections are extracted from the second simulated cardiac cycle. This decision was mainly driven by the computational cost of the simulations; however, in Figure 8, top, we show the periodicity of the inlet flow rate for both P1 and P2 in the Pre-PVR, Post-PVR and Follow-up scenarios.

In Table 5, we provide an overview of the main settings used for the simulations in the three scenarios.

4.2 | Velocity and pressure analysis

We start the discussion of the results by analysing systolic blood flow velocities for the Pre-PVR and Follow-up scenarios; specifically, we observe the instant characterised by the maximum blood velocity. In the velocity plots of Figure 9, left, we notice that the blood velocity is higher in the Follow-up scenario than in the Pre-PVR. In particular, after the valve implantation, the peak velocity in the pulmonary artery reaches 130 cm/s; this value is higher than the physiological range of 60–100 cm/s,[66] however, it can be found in patients with hypertrophy of the right heart, a condition which

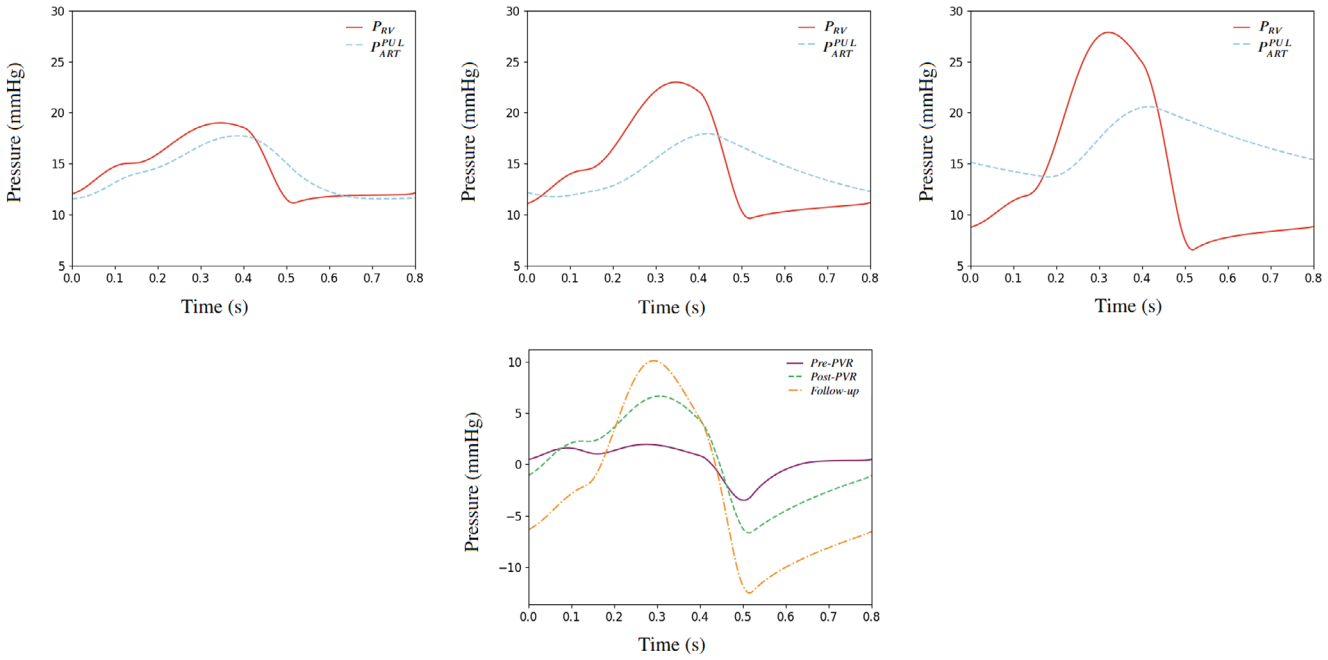

FIGURE 7 Top: Time-varying pressure boundary conditions computed by the 0D model and prescribed at the inlet (P^{RV}) and at the outlets (P_{ART}^{PUL}) of the 3D rFSI model for the three scenarios: Pre-PVR (left), Post-PVR (middle), Follow-up (right); Bottom: Corresponding pressure drops between the right ventricle and pulmonary artery compartments ($P^{RV} - P_{ART}^{PUL}$) in the three simulated scenarios.

commonly affects patients that have suffered from Tetralogy of Fallot, as those analysed in the present work.[67] Moreover, we notice that the different points of impact of the fluid jet on the artery wall in P1's and P2's velocity plots (in Follow-up scenarios) put in evidence the effect of the pulmonary artery geometry and valve orientation on the velocity pattern.

As for the diastolic velocity field and flow rates (see Figure 9, right), we observe that in the Follow-up scenario the closure of the valve prevents regurgitation, which occurs instead in the Pre-PVR scenario due to the valve absence. In Table 6 we report the computed synthetic flow rate indicators, namely the right ventricle total Ejected Volume (EV), the Regurgitant Volume (RV) – defined as the volume that returns to the ventricle when the backflow is established – and the Stroke Volume SV = EV − RV, for the 3D rFSI simulations. By computing the Regurgitant Fraction $RF = (RV/EV) \cdot 100$, which is commonly used as a measure of pulmonary insufficiency, we obtain $RF = 39.4\%$ and $RF = 41.4\%$ in the Pre-PVR scenarios. From these results, we notice that about 40% of the blood ejected by the right ventricle during the cardiac cycle returns into the ventricle. The values found are coherent with the literature; in particular, a regurgitant fraction of 40% coincides with the condition of pulmonary valve severe insufficiency and constitutes an indication for pulmonary valve replacement.[68] On the contrary, in the Follow-up scenario, we notice a significant reduction in the RV, as expected after the valve implantation. Moreover, we observe that SV is only slightly reduced after the valve implantation.

In Figure 8, bottom, we display the time evolution of flow rate through the valvular plane in time. We observe that the values of flow rate exiting the ventricle (positive values) reach a systolic peak of approximately 200 ml/s, coherent with the reference values for the pulmonary artery flow rate found in the literature.[69]

To highlight the effects of considering a 3D model of the pulmonary artery and valve, we compare the flow rate results at the valvular plane obtained by means of the rFSI simulations with those of the LPM. In Table 6 we report the synthetic flow indicators obtained from the LPM simulation: a larger EV and smaller RV are observed with respect to the corresponding rFSI values, thus yielding a smaller regurgitant fraction. This is also confirmed by the flow rate time evolution reported in Figure 10. We observe that in the Pre-PVR scenario (see Figure 10, left), the instantaneously opening diode in the LPM allows for a very rapidly increasing flow rate in the early systole, whereas in the rFSI model the flow inertia leads to a more gradual flow rate increase, which results in a reduced ejected volume. Instead, in the Follow-up scenario (see Figure 10, right), the use of an instantaneously closing diode in the LPM simulation prevents capturing any regurgitation, which is present in the rFSI case. Furthermore, we observe a larger flow rate peak in the

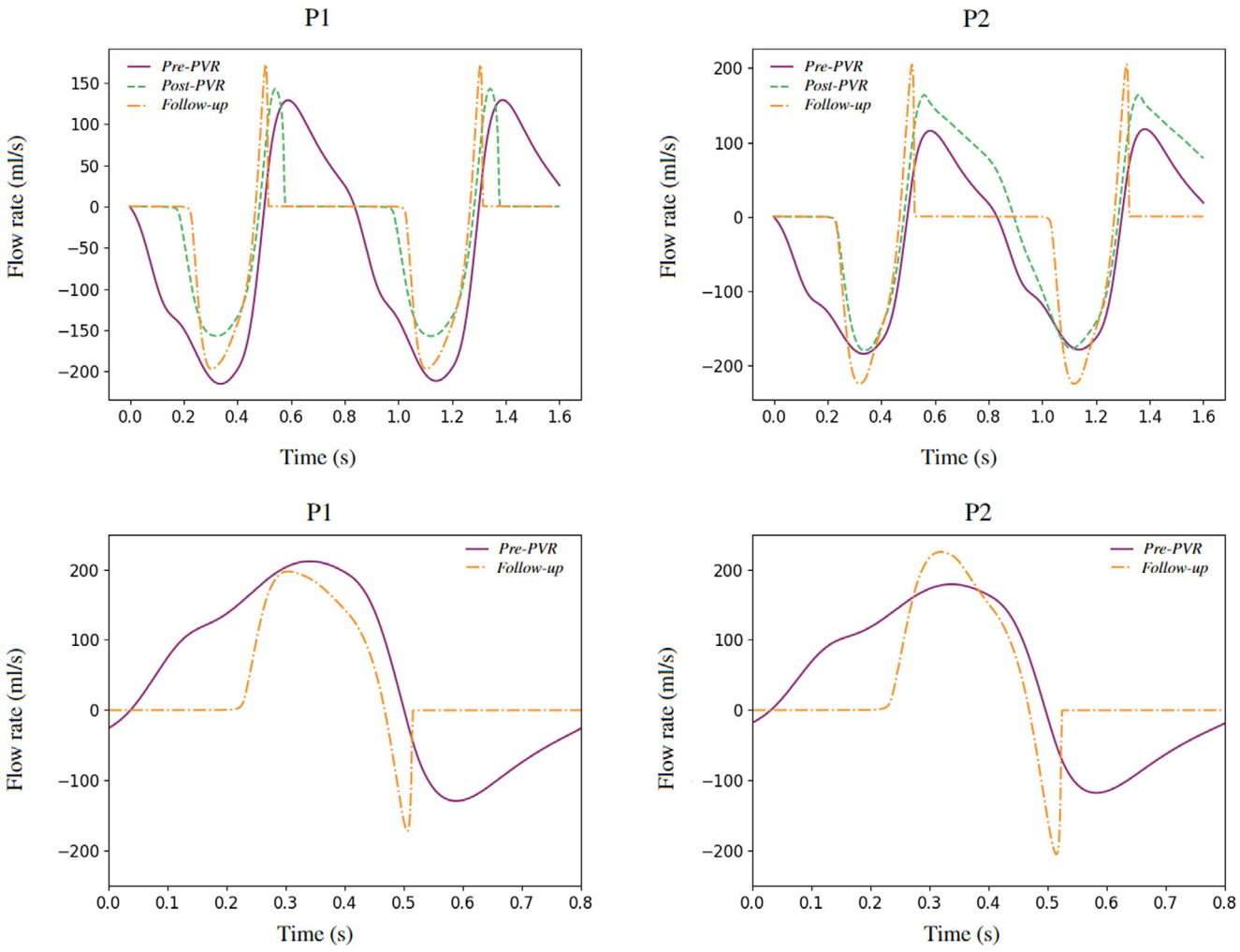

FIGURE 8 Top: Flow rate periodicity at the inlet section in the two cardiac cycles simulated with the rFSI model in the Pre-PVR, Post-PVR and Follow-up scenarios. Bottom: P1 and P2's flow rate through the valvular plane in the Pre-PVR and Follow-up simulated scenarios.

TABLE 5 Synthesis of both P1's and P2's configuration of the three scenarios considered for the numerical simulations.

	Pre-PVR	**Post-PVR**	**Follow-up**
Geometry	Absent valve	Stent graft inserted Valve included	Stent graft inserted Valve included
Data used for LPM calibration	6 months after PVR	6 months after PVR	9 years after PVR
RIIS term resistance	$R = 0\,\mathrm{kg\,m^{-1}\,s^{-1}}$	$R = 10^4\,\mathrm{kg\,m^{-1}\,s^{-1}}$	$R = 10^4\,\mathrm{kg\,m^{-1}\,s^{-1}}$
LPM valve resistances	$R_{max} = R_{min}$	$R_{max} >> R_{min}$	$R_{max} >> R_{min}$

LPM results: the reason for this is that the LPM does not account for the valve encumbrance. All these observations justify the use of a 3D model instead of LPM to describe specific haemodynamic features close to the valve.

In Figure 11 we show the plots of the diastolic pressure for Pre-PVR, Post-PVR and Follow-up scenarios of the two patients. We notice that the pressure values are close to the physiological range, especially in the Follow-up scenario.[70] In this scenario, we can see how the closed valve sustains a significant pressure drop (see zoom in Figure 11). This effect is less evident in the Post-PVR scenario, due to the lower pressure drop assigned through the boundary conditions. On the other end, in the Pre-PVR scenario the valve absence prevents the formation of a significant pressure gradient throughout the whole geometry.

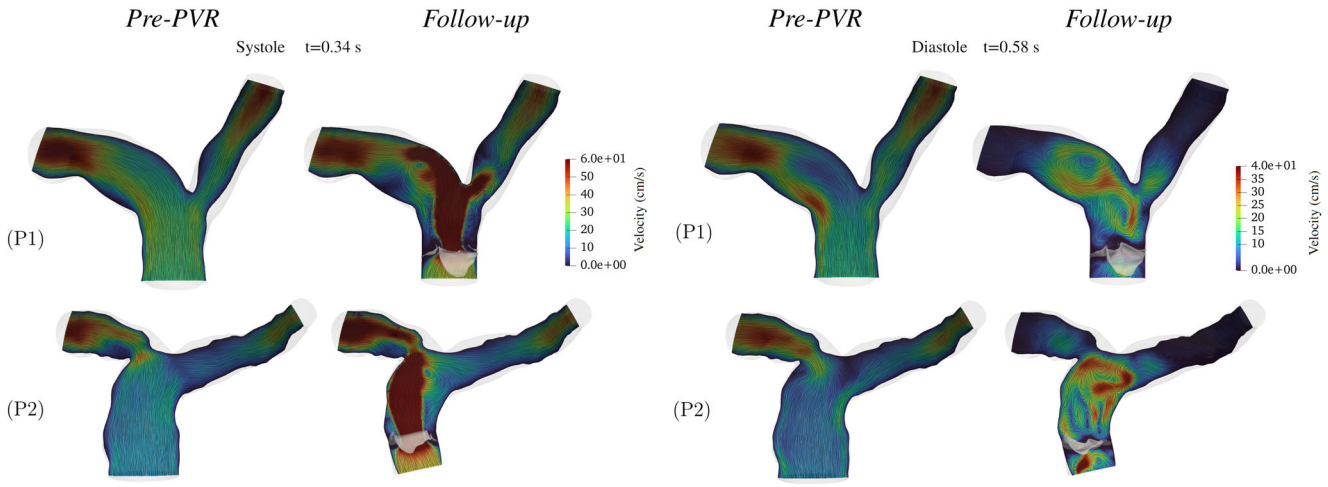

FIGURE 9 P1 and P2's velocity field in the Pre-PVR and Follow-up scenarios at t = 0.34 s (systolic phase) and at t = 0.58 s (diastolic phase).

TABLE 6 Values of EV, RV and SV computed in the 3D simulations of the Pre-PVR and Follow-up scenarios for P1 and P2 and in the LPM.

	P1—3D rFSI		P2—3D rFSI		LPM	
	Pre-PVR	**Follow-up**	**Pre-PVR**	**Follow-up**	**Pre-PVR**	**Follow-up**
EV (ml)	63.9	33.3	54.3	35.3	83.0	75.1
RV (ml)	25.2	4.7	22.5	6.6	15.4	0.0
SV (ml)	38.7	28.6	31.8	28.7	67.6	75.1

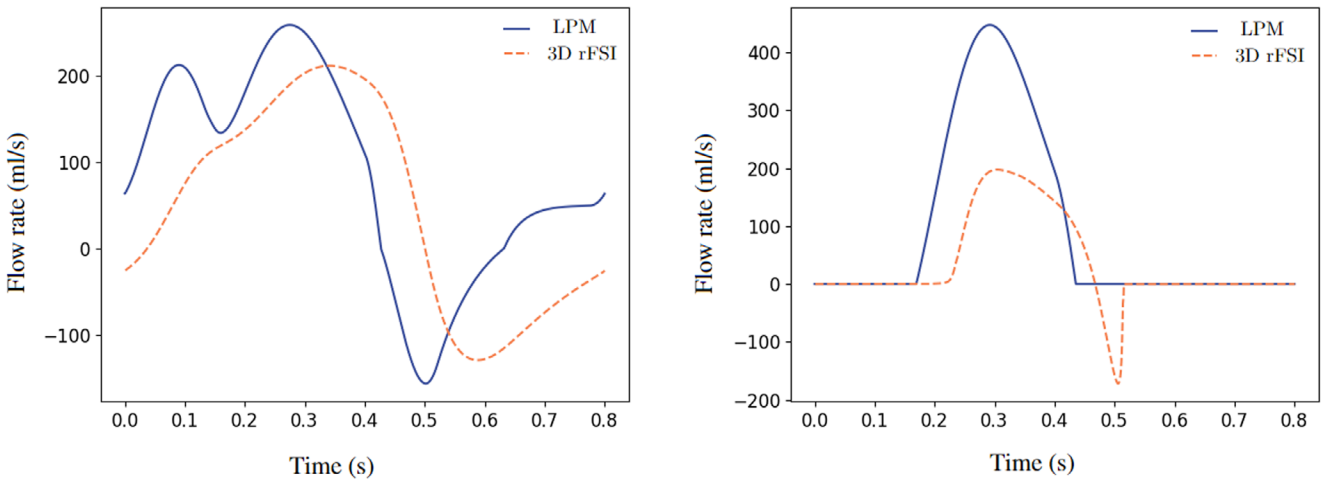

FIGURE 10 Comparison between LPM and P1 3D rFSI flow rates through the valvular plane, in the Pre-PVR (left) and Follow-up (right) scenarios.

4.3 | Wall shear stress and turbulence analysis

From the velocity field we derive the Wall Shear Stress (WSS), namely the tangential force per unit area that is applied by the blood flowing on the surface of the pulmonary wall (Γ_{wall}), defined as[71]:

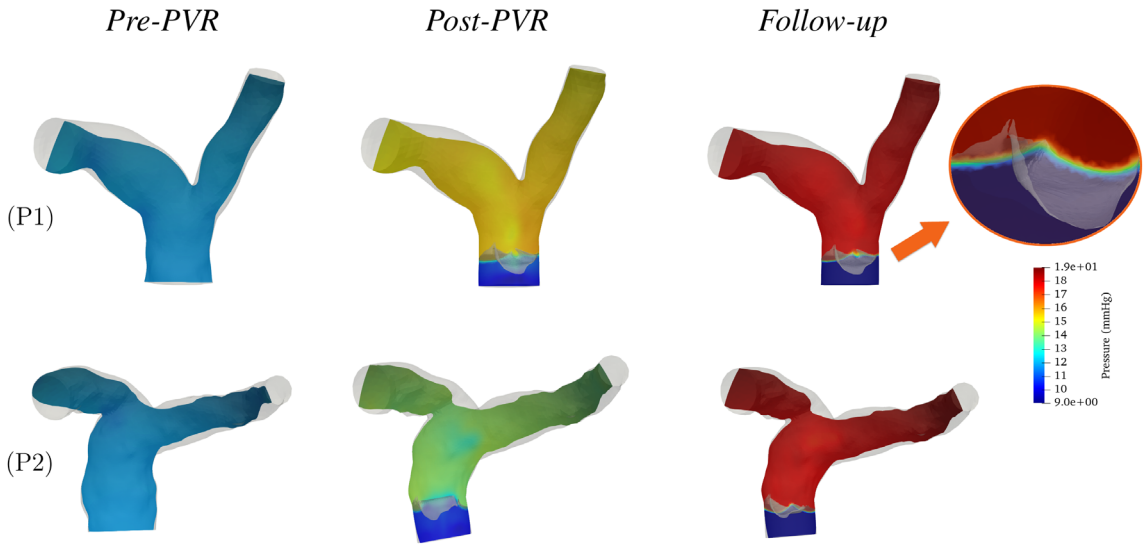

FIGURE 11 P1's and P2's pressure plots in the three simulated scenarios at the diastolic time t = 0.58 s.

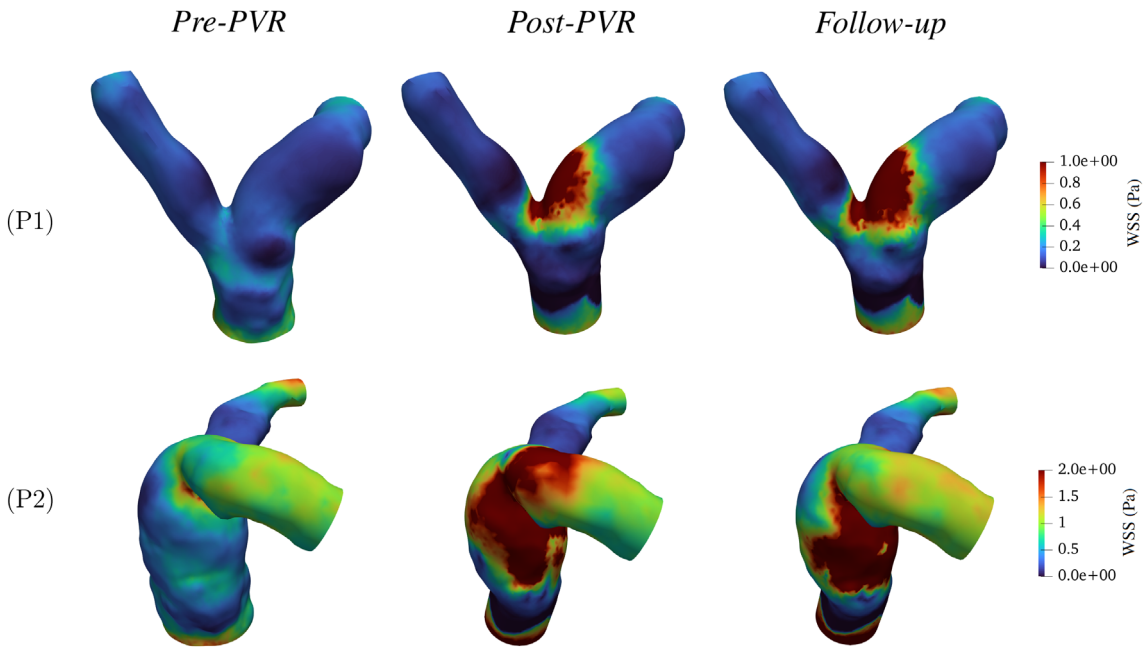

FIGURE 12 P1's and P2's Wall Shear Stress in the three simulated scenarios during the systolic phase (t = 0.34 s).

$$\mathrm{WSS} = \left(\mu + \mu_{sgs}\right) \sqrt{\sum_{j=1}^{2} \left[\left(\nabla \mathbf{u} + \nabla \mathbf{u}^T\right) \mathbf{n} \cdot \boldsymbol{\tau}_j\right]^2} \quad \text{on } \Gamma_{wall},$$

where $\boldsymbol{\tau}_j, j = 1,2$, are the tangential unit vectors. We report the result in Figure 12, where we notice that the prosthetic valve significantly affects the distribution of the WSS along the artery wall. In particular, we notice that the WSS is higher in the Post-PVR and Follow-up scenarios, due to the higher velocity of the blood. Moreover, for these scenarios, high values of WSS identify the impingement region of the systolic jet, which is different between the patients due to the different geometries and valve orientations. This observation is consistent with those on the systolic velocity profiles reported in Section 4.2. In the literature, low (and oscillatory) WSS is considered a risk factor for possible endothelium damage and atherosclerotic plaque formation.[72] It has been also recently associated with structural valve deterioration, which is a long-term risk for bioprosthetic valves like the one considered in the present study.[73,74] Our results show that

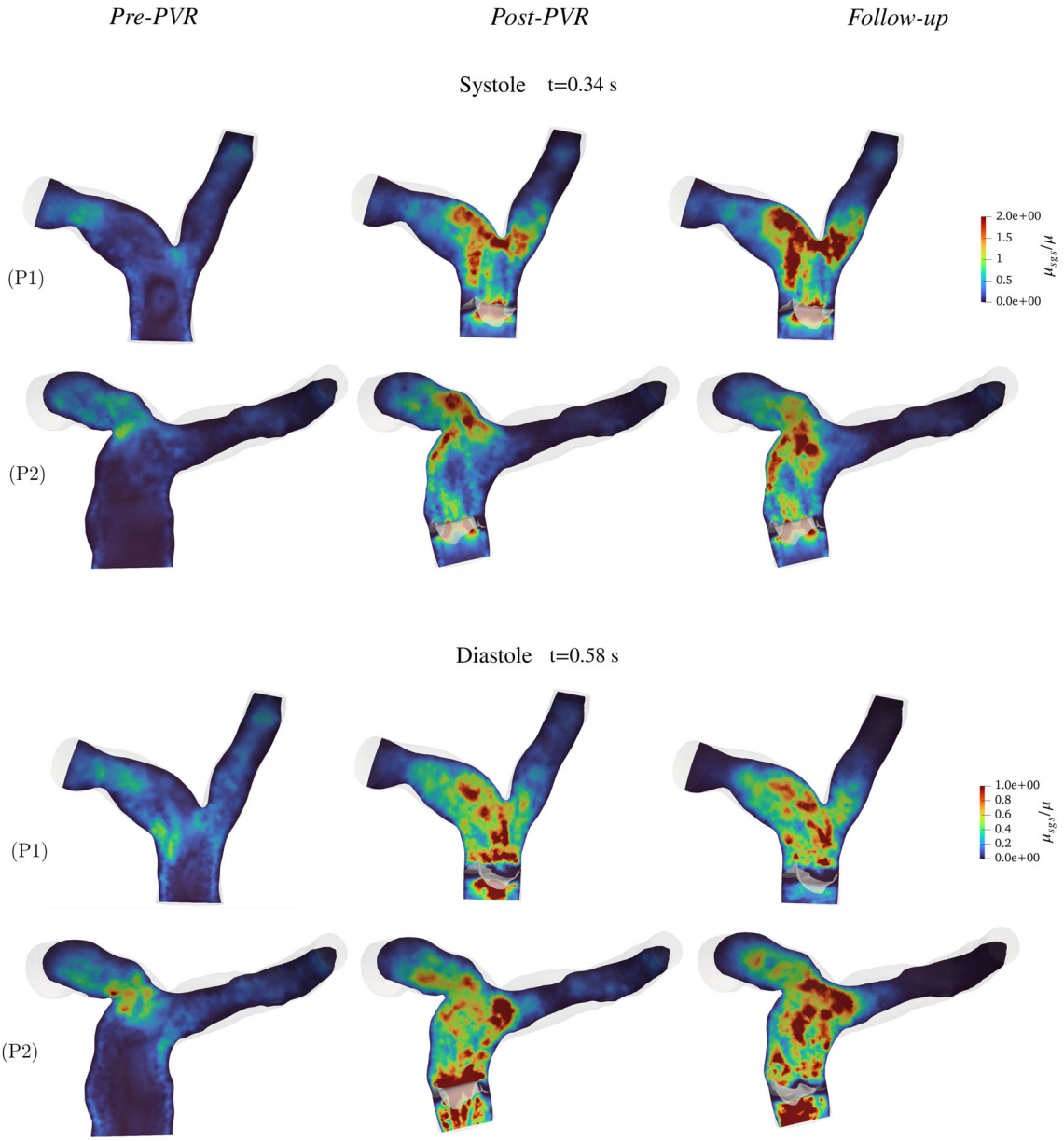

FIGURE 13 The ratio μ_{sgs}/μ for both P1 and P2 in the three scenarios analysed at time systolic time t = 0.34 s and diastolic time t = 0.58 s.

the virtual insertion of the pulmonary valve yields an increase in the WSS from the Pre-PVR to the Post-PVR and Follow-up scenarios, thus reducing the aforementioned risks. Specifically, the latter scenarios present WSS values in the physiological range reported by Tang, et al.[22]

In Figure 13 we display the turbulent viscosity ratio μ_{sgs}/μ, where μ_{sgs} is the turbulent viscosity of the LES σ-model; high values of μ_{sgs}/μ indicate a local regime of transition to turbulence.[39,40] We notice that the viscosity ratio is much smaller in Pre-PVR than Post-PVR and Follow-up. In the latter two scenarios, during systole (Figure 13, top) high values of μ_{sgs}/μ identify the vortices generated by the flow jet exiting the valve and its impact on the arterial wall. In diastole (Figure 13, bottom), μ_{sgs}/μ puts in evidence the vortex breaking in the artery.

5 | CONCLUDING REMARKS AND LIMITATIONS

In this work we have studied the haemodynamics in the pulmonary artery in presence of pulmonary valve replacement. To do this we use a reduced FSI model based on the interaction between a 3D FSI and a 1-DoF valve model, here applied for the first time to a patient-specific scenario.

The major outcomes of the study are:

- The proposed rFSI model was able to reproduce overall physiological and/or pathological conditions, as preliminary assessed on two different patients, for which we could calibrate the model hinging upon limited clinical measures. For these patients, the model allowed to verify the effects of the valve implantation on the pulmonary artery fluid dynamics;
- The LPM and rFSI model calibrated on patient P1's data could be effectively employed in the analysis of patient P2, namely it reproduced pulmonary artery haemodynamic conditions consistent with the literature and this patient's pathology, without the need for re-calibration;
- In the Post-PVR and Follow-up scenarios, the valve in the rFSI model rapidly closed during the early diastole and then sustained an inverse pressure gradient without regurgitation throughout the whole diastolic phase. In accordance with clinical observations on PVR patients, the transvalvular pressure gradient is slightly larger in Follow-up than in Post-PVR;
- As expected, the Post-PVR and Follow-up scenarios were characterised by larger values of velocity field, WSS, and turbulence, yet in a range in accordance with Tetralogy of Fallot patients.

We highlight some of the limitations encountered during the study:

- For P2, geometrical data were provided, but we lacked clinical haemodynamics measures. The validation against measures of other patients should be performed in future studies in order to further assess the robustness of our calibration;
- In absence of specific data, we calibrated the Pre-PVR LPM using the Post-PVR EF, ESV and EDV. Although, as observed in Section 3.3.1, the global quantities used in the calibration could not change that much,[60] immediately after PVR the after-load changes and the volume-overload of the RV is also reduced. Thus, pre-operative data would be needed for a future investigation on Pre-PVR LPM calibration;
- The computed Follow-up flow rate across the valve showed to be characterised by a non-negligible level of regurgitation. Although the latter is in accordance with the patients' conditions, for future studies we need to better assess the rFSI model to reduce such effect;
- The choice of a One-Way coupling between the 3D model and the LPM introduces a splitting error with respect to a Two-Way coupling; however, this represents a mild limitation which should not imply a substantial change in the main results of the paper. Indeed, previous works on pulmonary haemodynamics show that the results obtained with the Two-Way and the One-Way coupling are comparable[30];
- The LPM does not consider different compartments for the two pulmonary artery branches; thus, the same boundary condition is prescribed to 3D model at the two outlets. A further enhancement of the model should consider two different LPM outlet compartments, accounting for an uneven flow between the arterial branches. This would require the calibration of further model parameters.

ACKNOWLEDGEMENTS

IF has received support from ICSC–Centro Nazionale di Ricerca in High Performance Computing, Big Data, and Quantum Computing funded by European Union–NextGenerationEU, and from grant No. 740132, iHEART—An Integrated Heart Model for the simulation of the cardiac function, P.I. Prof. A. Quarteroni, funded by the European Research Council (ERC) under the European Union's Horizon 2020 research and innovation program. CV has been partially supported by the Italian Ministry of University and Research (MIUR) within the PRIN (Research projects of relevant national interest) MIUR PRIN22-PNRR n. P20223KSS2 "Machine learning for fluid-structure interaction in cardiovascular problems: efficient solutions, model reduction, inverse problems", and by the Italian Ministry of Health within the PNC PROGETTO HUB LIFE SCIENCE—DIAGNOSTICA AVANZATA (HLS-DA) "INNOVA", PNC-E3-2022-23683266–CUP: D43C22004930001, within the "Piano Nazionale Complementare Ecosistema Innovativo della Salute"—Codice univoco investimento: PNC-E3-2022-23683266. The present research is part of the activities of the project Dipartimento di Eccellenza 2023–2027, Dipartimento di Matematica, Politecnico di Milano. EC, IF and CV are members of the INdAM group GNCS "Gruppo Nazionale per il Calcolo Scientifico" (National Group for Scientific Computing).

DATA AVAILABILITY STATEMENT

The data that support the findings of this study are available on request from the corresponding author. The data are not publicly available due to privacy or ethical restrictions.

ORCID

Ivan Fumagalli https://orcid.org/0000-0001-9256-1398
Alfio Quarteroni https://orcid.org/0000-0002-5947-6885
Christian Vergara https://orcid.org/0000-0001-9872-5410

ENDNOTE

[i] Notice that with "reduced", here we mean that the model is given by using a 1-DoF valve model rather than a 3D one. As a consequence, we stress that we are not considering reduced order modelling, nor a lumped-parameter diode representation.

REFERENCES

1. Kidane AG, Burriesci G, Cornejo P, et al. Current developments and future prospects for heart valve replacement therapy. *J Biomed Mater Res B Appl Biomater*. 2009;88(1):290-303.
2. Fioretta ES, Dijkman PE, Emmert MY, Hoerstrup SP. The future of heart valve replacement: recent developments and translational challenges for heart valve tissue engineering. *J Tissue Eng Regen Med*. 2018;12(1):e323-e335.
3. Nestola MG, Zulian P, Gaedke-Merzhäuser L, Krause R. Fully coupled dynamic simulations of bioprosthetic aortic valves based on an embedded strategy for fluid–structure interaction with contact. *EP Europace*. 2021;23(Supplement_1):i96-i104.
4. Goldstone AB, Chiu P, Baiocchi M, et al. Mechanical or biologic prostheses for aortic-valve and mitral-valve replacement. *N Engl J Med*. 2017;377(19):1847-1857.
5. Head SJ, Çelik M, Kappetein AP. Mechanical versus bioprosthetic aortic valve replacement. *Eur Heart J*. 2017;38(28):2183-2191.
6. Morganti S, Conti M, Aiello M, et al. Simulation of transcatheter aortic valve implantation through patient-specific finite element analysis: two clinical cases. *J Biomech*. 2014;47(11):2547-2555.
7. Gillinov AM, Blackstone EH, Nowicki ER, et al. Valve repair versus valve replacement for degenerative mitral valve disease. *J Thorac Cardiovasc Surg*. 2008;135(4):885-893.
8. Diaz-Frias J, Guillaume M. *Tetralogy of Fallot*. StatPearls Publishing; 2022.
9. Apitz C, Webb GD, Redington AN. Tetralogy of Fallot. *Lancet*. 2009;374(9699):1462-1471.
10. Forman J, Beech R, Slugantz L, Donnellan A. A review of tetralogy of Fallot and postoperative management. *Crit Care Nurs Clin North Am*. 2019;31(3):315-328.
11. Sharkey AM, Sharma A. *Tetralogy of Fallot: anatomic variants and their impact on surgical management*. 16. SAGE Publications Sage CA; 2012:88-96.
12. European Paediatric Cardiology (AEPC) b. t. A. fE, Members AF, Baumgartner H, et al. ESC guidelines for the management of grown-up congenital heart disease (new version 2010) the task force on the Management of Grown-up Congenital Heart Disease of the European Society of Cardiology (ESC). *Eur Heart J*. 2010;31(23):2915-2957.
13. Artemiou P, Schusterova I, Tohatyova A, Cocherova J, Krcho P, Sabol F. Follow-up after the Ross procedure, how significant it is, case reports of three patients. *J Cardiothorac Surg*. 2015;10:1-4.
14. Ghitti B, Toro EF, Müller LO. Nonlinear lumped-parameter models for blood flow simulations in networks of vessels. *ESAIM: Mathematical Modelling and Numerical Analysis*. 2022;56(5):1579-1627.
15. Quarteroni A, Veneziani A, Vergara C. Geometric multiscale modeling of the cardiovascular system, between theory and practice. *Comput Methods Appl Mech Eng*. 2016;302:193-252.
16. Kim HJ, Vignon-Clementel IE, Figueroa CA, et al. On coupling a lumped parameter heart model and a three-dimensional finite element aorta model. *Ann Biomed Eng*. 2009;37:2153-2169.
17. Shimizu S, Une D, Kawada T, et al. Lumped parameter model for hemodynamic simulation of congenital heart diseases. *J Physiol Sci*. 2018;68:103-111.
18. Trenhago PR, Fernandes LG, Müller LO, Blanco PJ, Feijóo RA. An integrated mathematical model of the cardiovascular and respiratory systems. *Int J Numer Methods Biomed Eng*. 2016;32(1):e02736.
19. Kilner PJ, Balossino R, Dubini G, et al. Pulmonary regurgitation: the effects of varying pulmonary artery compliance, and of increased resistance proximal or distal to the compliance. *Int J Cardiol*. 2009;133(2):157-166.
20. Boileau E, Nithiarasu P, Blanco PJ, et al. A benchmark study of numerical schemes for one-dimensional arterial blood flow modelling. *Int J Numer Methods Biomed Eng*. 2015;31(10):e02732.
21. Tang BT, Fonte TA, Chan FP, Tsao PS, Feinstein JA, Taylor CA. Three-dimensional hemodynamics in the human pulmonary arteries under resting and exercise conditions. *Ann Biomed Eng*. 2011;39:347-358.
22. Tang BT, Pickard SS, Chan FP, Tsao PS, Taylor CA, Feinstein JA. Wall shear stress is decreased in the pulmonary arteries of patients with pulmonary arterial hypertension: an image-based, computational fluid dynamics study. *Pulm Circ*. 2012;2(4):470-476.

23. Boumpouli M, Sauvage EL, Capelli C, Schievano S, Kazakidi A. Characterization of flow dynamics in the pulmonary bifurcation of patients with repaired tetralogy of fallot: a computational approach. *Front Cardiovasc Med*. 2021;8:703717.
24. Aslan S, Guillot M, Ross-Ascuitto N, Ascuitto R. Hemodynamics in a bidirectional Glenn shunt supplemented with a modified Blalock-Taussig shunt: computational fluid dynamics assessment. *Prog Pediatr Cardiol*. 2021;60:101256.
25. Vignon-Clementel IE, Marsden AL, Feinstein JA. A primer on computational simulation in congenital heart disease for the clinician. *Prog Pediatr Cardiol*. 2010;30(1–2):3-13.
26. Baretta A, Corsini C, Yang W, et al. Virtual surgeries in patients with congenital heart disease: a multi-scale modelling test case. *Philos Trans R Soc A Math Phys Eng Sci*. 1954;2011(369):4316-4330.
27. Corsini C, Cosentino D, Pennati G, Dubini G, Hsia TY, Migliavacca F. Multiscale models of the hybrid palliation for hypoplastic left heart syndrome. *J Biomech*. 2011;44(4):767-770.
28. Aghilinejad A, Amlani F, Mazandarani SP, King KS, Pahlevan NM. Mechanistic insights on age-related changes in heart-aorta-brain hemodynamic coupling using a pulse wave model of the entire circulatory system. *Am J Phys Heart Circ Phys*. 2023;325(5):H1193-H1209.
29. Mynard JP, Smolich JJ. One-dimensional haemodynamic modeling and wave dynamics in the entire adult circulation. *Ann Biomed Eng*. 2015;43:1443-1460.
30. Marcinno' F, Zingaro A, Fumagalli I, Dede' L, Vergara C. A computational study of blood flow dynamics in the pulmonary arteries. *Vietnam J Math*. 2023;51(1):127-149.
31. Liu J, Yang W, Lan IS, Marsden AL. Fluid-structure interaction modeling of blood flow in the pulmonary arteries using the unified continuum and variational multiscale formulation. *Mech Res Commun*. 2020;107:103556.
32. Kong F, Kheyfets V, Finol E, Cai XC. Simulation of unsteady blood flows in a patient-specific compliant pulmonary artery with a highly parallel monolithically coupled fluid-structure interaction algorithm. *Int J Numer Methods Biomed Eng*. 2019;35(7):e3208.
33. Yang W, Dong M, Rabinovitch M, Chan FP, Marsden AL, Feinstein JA. Evolution of hemodynamic forces in the pulmonary tree with progressively worsening pulmonary arterial hypertension in pediatric patients. *Biomech Model Mechanobiol*. 2019;18(3):779-796.
34. Zambrano BA, McLean N, Zhao X, et al. Patient-specific computational analysis of hemodynamics and wall mechanics and their interactions in pulmonary arterial hypertension. *Front Bioeng Biotechnol*. 2021;8:611149.
35. Fumagalli I. A reduced 3D-0D FSI model of the aortic valve including leaflets curvature. *arXiv preprint arXiv:2106.00571*. 2021.
36. Capuano F, Loke YH, Balaras E. Blood flow dynamics at the pulmonary artery bifurcation. *Fluids*. 2019;4(4):190.
37. Montevecchi FM, Redaelli A. *Biomeccanica: analisi multiscala di tessuti biologici*. Pàtron. 2012:392.
38. Bessonov N, Sequeira A, Simakov S, Vassilevskii Y, Volpert V. Methods of blood flow modelling. *Math Modell Nat Phenom*. 2016;11(1):1-25.
39. Nicoud F, Toda HB, Cabrit O, Bose S, Lee J. Using singular values to build a subgrid-scale model for large eddy simulations. *Phys Fluids*. 2011;23(8):085106-01-085106-12.
40. Lancellotti RM, Vergara C, Valdettaro L, Bose S, Quarteroni A. Large eddy simulations for blood dynamics in realistic stenotic carotids. *Int J Numer Methods Biomed Eng*. 2017;33(11):e2868.
41. Bennati L, Vergara C, Giambruno V, et al. An image-based computational fluid dynamics study of mitral regurgitation in presence of prolapse. *Cardiovasc Eng Technol*. 2023;14:1-19.
42. Fernández MA, Gerbeau JF, Martin V. Numerical simulation of blood flows through a porous interface. *ESAIM: Mathematical Modelling and Numerical Analysis*. 2008;42(6):961-990.
43. Fedele M, Faggiano E, Dedè L, Quarteroni A. A patient-specific aortic valve model based on moving resistive immersed implicit surfaces. *Biomech Model Mechanobiol*. 2017;16:1779-1803.
44. Fumagalli I, Fedele M, Vergara C, et al. An image-based computational hemodynamics study of the systolic anterior motion of the mitral valve. *Comput Biol Med*. 2020;123:103922.
45. Quarteroni A, Sacco R, Saleri F. *Numerical Mathematics*. Vol 37. Springer Science & Business Media; 2010.
46. Bazilevs Y, Calo V, Cottrell J, Hughes T, Reali A, Scovazzi G. Variational multiscale residual-based turbulence modeling for large eddy simulation of incompressible flows. *Comput Methods Appl Mech Eng*. 2007;197(1–4):173-201.
47. Forti D, Dedè L. Semi-implicit BDF time discretization of the Navier–stokes equations with VMS-LES modeling in a high performance computing framework. *Comput Fluids*. 2015;117:168-182.
48. Africa PC, Fumagalli I, Bucelli M, et al. lifex-cfd: An Open-Source Computational Fluid Dynamics Solver for Cardiovascular Applications. *Computer Physics Communication*. 2024;296:109039.
49. Africa PC. lifex: a flexible, high performance library for the numerical solution of complex finite element problems. *SoftwareX*. 2022;20:101252.
50. Official website. https://lifex.gitlab.io/
51. Blanco PJ, Feijóo RA. A 3D-1D-0D computational model for the entire cardiovascular system. *Mecánica Computacional*. 2010;29(59):5887-5911.
52. Regazzoni F, Salvador M, Africa PC, Fedele M, Dedè L, Quarteroni A. A cardiac electromechanical model coupled with a lumped-parameter model for closed-loop blood circulation. *J Comput Phys*. 2022;457:111083.
53. Hemalatha K, Manivannan M. A study of cardiopulmonary interaction haemodynamics with detailed lumped parameter model. *Int J Biomed Eng Technol*. 2011;6(3):251-271.
54. Ghiselli S, Carro C, Uricchio N, Annoni G, Marianeschi SM. Mid-to long-term follow-up of pulmonary valve replacement with Bio-Integral injectable valve. *Eur J Cardiothorac Surg*. 2021;59(2):325-332.
55. VMTK. Vascular, Modeling, Toolkit. http://www.vmtk.org/index.html

56. Fedele M, Quarteroni A. Polygonal surface processing and mesh generation tools for the numerical simulation of the cardiac function. *Int J Numer Methods Biomed Eng*. 2021;37(4):e3435.
57. Paraview. https://www.paraview.org/
58. Zygote. http://www.zygote.com
59. Wang S, Wang S, Zhu Q, et al. Reference values of right ventricular volumes and ejection fraction by three-dimensional echocardiography in adults: a systematic review and meta-analysis. *Front Cardiovasc Med*. 2021;8:709863.
60. Geva T, Gauvreau K, Powell AJ, et al. Randomized trial of pulmonary valve replacement with and without right ventricular remodeling surgery. *Circulation*. 2010;122(11_suppl_1):S201-S208.
61. Lang RM, Badano LP, Mor-Avi V, et al. Recommendations for cardiac chamber quantification by echocardiography in adults: an update from the American Society of Echocardiography and the European Association of Cardiovascular Imaging. *Eur Heart J Cardiovasc Imaging*. 2015;16(3):233-271.
62. Keenon A, Crouch ED, Faber JE, Stouffer GA. Normal hemodynamics. In: Stouffer GA, Klein JL, McLaughlin DP (eds). *Cardiovasc Hemodynamics Clinician*. John Wiley & Sons; 2017;37-55.
63. Tasca G, Vismara R, Trinca F, Riva B, Gamba A, Lobiati E. Opening/closing pattern of trifecta and freestyle valves versus native aortic valve: are stentless valves more physiologic than a stented valve? *J Card Surg*. 2017;32:680-685. doi:10.1111/jocs.13231
64. Handke M, Heinrichs G, Beyersdorf F, Olschewski M, Bode C, Geibel A. In vivo analysis of aortic valve dynamics by transesophageal 3-dimensional echocardiography with high temporal resolution. *J Thorac Cardiovasc Surg*. 2003;125(6):1412-1419.
65. This A, Morales HG, Bonnefous O, Fernández MA, Gerbeau JF. A pipeline for image based intracardiac CFD modeling and application to the evaluation of the PISA method. *Comput Methods Appl Mech Eng*. 2020;358:112627.
66. Bouhemad B, Ferrari F, Leleu K, Arbelot C, Lu Q, Rouby JJ. Echocardiographic Doppler estimation of pulmonary artery pressure in critically ill patients with severe hypoxemia. *J Am Soc Anesthesiologists*. 2008;108(1):55-62.
67. Grotenhuis HB, Kroft LJ, Elderen vSG, et al. Right ventricular hypertrophy and diastolic dysfunction in arterial switch patients without pulmonary artery stenosis. *Heart*. 2007;93(12):1604-1608.
68. Frigiola A, Tsang V, Nordmeyer J, et al. Current approaches to pulmonary regurgitation. *Eur J Cardiothorac Surg*. 2008;34:576-581. doi: 10.1016/j.ejcts.2008.04.046
69. Wehrum T, Hagenlocher P, Lodemann T, et al. Age dependence of pulmonary artery blood flow measured by 4D flow cardiovascular magnetic resonance: results of a population-based study. *J Cardiovasc Magn Reson*. 2016;18:1-9.
70. Kovacs G, Berghold A, Scheidl S, Olschewski H. Pulmonary arterial pressure during rest and exercise in healthy subjects: a systematic review. *Eur Respir J*. 2009;34(4):888-894.
71. Quarteroni A, Manzoni A, Vergara C. The cardiovascular system: mathematical modelling, numerical algorithms and clinical applications. *Acta Numerica*. 2017;26:365-590. doi:10.1017/S0962492917000046
72. Peiffer V, Sherwin SJ, Weinberg PD. Does low and oscillatory wall shear stress correlate spatially with early atherosclerosis? *Syst Rev Cardiovasc Res*. 2013;99(2):242-250.
73. Fumagalli I, Polidori R, Renzi F, et al. Fluid-structure interaction analysis of transcatheter aortic valve implantation. *Int J Numer Methods Biomed Eng*. 2023;39(6):e3704.
74. Chen PC, Sager MS, Zurakowski D, et al. Younger age and valve oversizing are predictors of structural valve deterioration after pulmonary valve replacement in patients with tetralogy of Fallot. *J Thorac Cardiovasc Surg*. 2012;143(2):352-360.

How to cite this article: Criseo E, Fumagalli I, Quarteroni A, Marianeschi SM, Vergara C. Computational haemodynamics for pulmonary valve replacement by means of a reduced fluid-structure interaction model. *Int J Numer Meth Biomed Engng*. 2024;40(9):e3846. doi:10.1002/cnm.3846